# Photoreceptor and Retinal Pigment Epithelium Relationships in Eyes With Vitelliform Macular Dystrophy Revealed by Multimodal Adaptive Optics Imaging

Tao Liu[1], Nancy Aguilera[1], Andrew J. Bower[1], Joanne Li[1], Ehsan Ullah[1], Alfredo Dubra[2], Catherine Cukras,[1] Brian P. Brooks[1], Brett G. Jeffrey[1], Robert B. Hufnagel[1], Laryssa A. Huryn[1], Wadih M. Zein[1], and Johnny Tam[1]

[1]National Eye Institute, National Institutes of Health, Bethesda, Maryland, United States
[2]Department of Ophthalmology, Stanford University, Palo Alto, California, United States

Correspondence: Johnny Tam, National Eye Institute, National Institutes of Health, 10 Center Drive, Room 10N109, Bethesda, MD 20892, USA;
johnny@nih.gov.

**Received:** January 21, 2022
**Accepted:** June 16, 2022
**Published:** July 28, 2022

Citation: Liu T, Aguilera N, Bower AJ, et al. Photoreceptor and retinal pigment epithelium relationships in eyes with vitelliform macular dystrophy revealed by multimodal adaptive optics imaging. *Invest Ophthalmol Vis Sci.* 2022;63(8):27. https://doi.org/10.1167/iovs.63.8.27

**Purpose.** To assess the structure of cone photoreceptors and retinal pigment epithelial (RPE) cells in vitelliform macular dystrophy (VMD) arising from various genetic etiologies.

**Methods.** Multimodal adaptive optics (AO) imaging was performed in 11 patients with VMD using a custom-assembled instrument. Non-confocal split detection and AO-enhanced indocyanine green were used to visualize the cone photoreceptor and RPE mosaics, respectively. Cone and RPE densities were measured and compared across *BEST1*-, *PRPH2*-, *IMPG1*-, and *IMPG2*-related VMD.

**Results.** Within macular lesions associated with VMD, both cone and RPE densities were reduced below normal, to 37% of normal cone density (eccentricity 0.2 mm) and to 8.4% of normal RPE density (eccentricity 0.5 mm). Outside of lesions, cone and RPE densities were slightly reduced (both to 92% of normal values), but with high degree of variability in the individual measurements. Comparison of juxtalesional cone and RPE measurements (<1 mm from the lesion edge) revealed significant differences in RPE density across the four genes ($P < 0.05$). Overall, cones were affected to a greater extent than RPE in patients with *IMPG1* and *IMPG2* pathogenic variants, but RPE was affected more than cones in *BEST1* and *PRPH2* VMD. This trend was observed even in contralateral eyes from a subset of five patients who presented with macular lesions in only one eye.

**Conclusions.** Assessment of cones and RPE in retinal locations outside of the macular lesions reveals a pattern of cone and RPE disruption that appears to be gene dependent in VMD. These findings provide insight into the cellular pathogenesis of disease in VMD.

Keywords: adaptive optics ophthalmoscopy, vitelliform macular dystrophy, photoreceptors, retinal pigment epithelium, indocyanine green

Vitelliform macular dystrophies (VMDs) are clinically defined by the presence of yellow domed macular lesion(s), resembling an "egg-yolk," that are present at a certain stage of disease and affect an estimated one in 5500 individuals.[1] The phenotypic appearance, initially based on ophthalmoscopic examination features, can be further refined by multimodal retinal imaging at different stages of disease.[2–7] Stage 1 (previtelliform) is associated with a normal-appearing fundus or subtle foveal pigment granularity. Stage 2 (vitelliform) is characterized by the presence of a yellow, elevated macular lesion that is hyperautofluorescent. On optical coherence tomography (OCT) an elevation of the retina with deposits separating the retinal pigment epithelial (RPE) cells and photoreceptors is noted. Stage 3 (pseudohypopyon) occurs with partial resorption of macular lesion fluid. Vision can remain relatively well preserved through this stage but declines by Stage 4 (vitelliruptive), where the lesion described in the previous stages appears to "scramble." Stages 5 and 6 (atrophy; cicatricial changes) can be associated with complications such as choroidal neovascularization.

Both clinical and genetic heterogeneity in the VMD phenotype have been reported. Although the disease is usually bilateral with a single lesion in the central macula, unilateral cases have been described,[8] and multifocal disease[9] can also occur. Pathogenic variants in *BEST1*, *PRPH2*, *IMPG1*, and *IMPG2* have all been associated with VMD, with *BEST1* noted most commonly. The expression of these genes is thought to differ across cell types (e.g., photoreceptors, RPE cells). The *BEST1* gene [Mendelian Inheritance in Man (MIM) #607854] encodes a bestrophin family protein expressed in RPE cells[10] that is believed to function as an anion channel and intracellular calcium signaling regulator[11,12] and is the gene most often associated with VMD.[13,14] In the case of *BEST1* related disease, dysfunction of the bestrophin protein leads to a weakened RPE-photoreceptor interface and formation of vitelliform deposits,[15] but histopathology has suggested that

Copyright 2022 The Authors


This work is licensed under a Creative Commons Attribution-NonCommercial-NoDerivatives 4.0 International License.

Downloaded from hwmaint.iovs.org on 04/24/2024

the affected area extends beyond the clinically-evident lesion.[16,17] Less commonly, *PRPH2* (MIM #179605), *IMPG1* (MIM #602870), and *IMPG2* (MIM #607056) have also been associated with VMD,[18–20] but the pathophysiology of vitelliform lesion development in these conditions is not well established. *PRPH2*, peripherin-2, encodes a tetraspanin transmembrane protein that localizes to the rims of cone lamellae and rod disks, where it helps maintain the structure and function of photoreceptor outer segments.[21,22] In addition to VMD, *PRPH2* is also associated with other retinal phenotypes including pattern macular dystrophy.[18] Finally, *IMPG1* (MIM #602870) and *IMPG2* (MIM #607056) encode two interphotoreceptor matrix proteoglycans that are important for the cone-specific glycocalyx and extracellular matrix surrounding cones.[23] Elucidating the cellular pathophysiology of VMD with respect to these different genes is an important first step toward unraveling the mechanisms of VMD.

Adaptive optics (AO) retinal imaging has been used to examine cone photoreceptor structure in patients with inherited retinal degenerations[24,25]; however, to date, there have been limited studies quantifying cone photoreceptor structure in VMD using AO. To our knowledge, only two quantitative AO reports assessing VMD have been reported, both in Best vitelliform macular dystrophy, revealing reduced cone density above macular lesions, but normal cone density outside of lesions.[26,27] Given that the vitelliform lesions arise at the interface between photoreceptors and RPE and that the genes associated with VMD encode proteins that span the photoreceptor-RPE interface, examination of the RPE mosaic alongside cone photoreceptors in VMD with differing genetic etiology is warranted. In this study, we demonstrate an application of multimodal AO imaging incorporating non-confocal split detection[28] and adaptive optics enhanced indocyanine green (AO-ICG) imaging[29,30] to investigate relationships between photoreceptors and RPE in a cohort of 11 patients with VMD associated with different genetic etiologies. Our results demonstrate the potential for using AO to help assess genotype-phenotype correlations.

## Methods

### Patients

Research procedures adhered to the tenets of the Declaration of Helsinki. Written informed consent was obtained after the nature of the research and possible consequences of the study were explained. The study was approved by the Institutional Review Board of the National Institutes of Health (NCT02317328). Patients diagnosed with at least one vitelliform macular lesion thought to be due to genetic etiology were recruited from the National Eye Institute eye clinic for adaptive optics retinal imaging. Patients who had unstable fixation or media opacity were excluded; for ICG, participants under 18 years of age or who were allergic to shellfish or iodine were also excluded. In addition, best-corrected visual acuity, dilated funduscopic examination, fundus photography (Topcon, Tokyo, Japan), fundus autofluorescence (Topcon or Spectralis, Heidelberg Engineering, Heidelberg, Germany) and optical coherence tomography (Spectralis, Heidelberg Engineering) were performed.

All patients underwent genetic testing from clinical genetic testing laboratories that used custom capture-based next-generation sequencing to sequence genes (minimum gene list = *ABCA4, BEST1, CDH3, EFEMP1, ELOVL4, IMPG1, IMPG2, PROM1, PRPH2*, *TIMP3*) involved in inherited macular dystrophies. Two patients, for whom initial testing was inconclusive, were subjected to larger custom-captured next-generation sequencing panels of 145 or 267 inherited retinal dystrophy genes. The variants were reanalyzed as per ACMG/AMP guidelines and reports were interpreted for genotype-phenotype correlation (Supplementary Table S1).

Full-field flash electroretinograms (ffERG) and electrooculograms (EOG) were recorded in a subset of patients according to the standards of the International Society for Clinical Electrophysiology Vision.[31,32] Briefly EOGs were recorded from skin electrodes placed on the outer and inner canthi of each eye and Arden ratio was used in analysis. The mean Arden ratio varies by age[33]; in this study the lower limit of normal Arden ratio ranged from 1.93 to 1.63 for the youngest to oldest subjects, respectively. After sitting in the dark for 30 minutes, scotopic ffERGs were then recoded from bipolar Burian-Allen contact lens electrodes. Subsequently, photopic ffERGs were recorded after 10 minutes of adaptation to a background of 30 cd/m$^2$. For both EOG and ffERG, a skin electrode attached to the forehead served as ground.

### Multimodal Adaptive Optics Imaging

A total of 20 eyes from 11 patients were imaged. Before imaging, eyes were dilated with 2.5% phenylephrine hydrochloride and 1% tropicamide. A custom-assembled multimodal AO retinal imager incorporating both non-confocal split detection[28] and AO-ICG[29,30] was used to acquire images from various retinal locations. Subjects were instructed to look at a fixation target, and breaks were taken when the operator observed degradation in fixational stability. The preferred retinal locus of fixation (PRL) was determined by asking subjects to look at the center of the dim red raster window of imaging light. Images of cone photoreceptors were obtained using non-confocal split detection (acquired both before and after ICG injection). RPE cells in 18 eyes (subject S8 declined ICG; see Table) were imaged using AO-ICG between 45 minutes to several hours after intravenous injection of indocyanine green (ICG) dye (25 mg in 3 mL). The imaging focus was set to the plane of best focus for photoreceptors. In eyes with macular lesions associated with VMD, multiple focal planes were captured above the lesions to bring the anteriorly displaced photoreceptors into focus. Approximately 50 to 100 overlapping locations were imaged per eye covering the macular lesions and a temporal strip of retina out to approximately 5.5 mm for cones and 2.5 mm for RPE.

### Image Analysis

Videos were postprocessed to correct for eye motion, using custom software.[34] Overlapping AO images containing co-registered split detection and AO-ICG images were assembled into montages and registered to clinical images. Square regions of interest (ROIs) were selected at various retinal locations avoiding medium and large blood vessels, with the size of each ROI adjusted to contain ~10 cells × ~10 cells.[35] For eyes with macular lesions, three categories of ROIs were selected: lesion, juxtalesion (within 1 mm of the lesion edge), and non-lesion areas outside of the juxtalesional area (out to an eccentricity of approximately 5.5 mm). For the lesion ROIs, if anteriorly-displaced photoreceptors were visible, two or three cone ROIs were selected per eye; if RPE cells were visible (typically only in resorbed areas), two RPE ROIs were selected per eye. For the juxtalesion ROIs, approximately 15 RPE ROIs were selected circumferentially

Investigative Ophthalmology & Visual Science

Downloaded from hwmaint.iovs.org on 04/24/2024

**Table.** Subject List

| ID[*] | F[†] | Age | Sex | Gene | Affected Eye[‡] | BCVA (OD, OS) | Stage[§] | Imaging[‖] | ffERG[#] | EOG[#] |
|---|---|---|---|---|---|---|---|---|---|---|
| S1 | F1 | 18 | F | *BEST1* | OD | 20/125 | Vitelliruptive | OD | — | OD |
| | | | | | — | 20/20 | Previtelliform | OS | — | OS |
| S2 | F2 | 19 | M | *BEST1* | OD | 20/63 | Atrophic | OD (*39*[**]) | OD | — |
| | | | | | — | 20/16 | Previtelliform | OS (*39*[**]) | OS | — |
| S3 | F2 | 19 | M | *BEST1* | OD | 20/40 | Vitelliruptive | OD (18) | OD | OD |
| | | | | | — | 20/12 | Previtelliform | OS (18) | OS | OS |
| S4 | F3 | 65 | M | *BEST1* | OD | 20/16 | Vitelliform | OD | OD | OD |
| | | | | | OS | 20/20 | Vitelliform | OS | OS | OS |
| S5 | F4 | 36 | F | *PRPH2* | OD | 20/25 | Vitelliform | OD (14) | OD | OD |
| | | | | | OS | 20/20 | Vitelliform | OS (14) | OS | OS |
| S6 | F5 | 50 | M | *PRPH2* | OD | 20/40 | Vitelliruptive, Multifocal | OD | OD | OD |
| | | | | | OS | 20/40 | Vitelliruptive, Multifocal | OS | OS | OS |
| S7 | F6 | 27 | M | *IMPG1* | — | 20/20 | Previtelliform | OD (9) | OD | OD |
| | | | | | OS | 20/32 | Pseudohypopyon, Multifocal | OS (9) | OS | OS |
| S8 | F6 | 60 | M | *IMPG1* | OD | 20/80 | Atrophic | OD | OD | OD |
| | | | | | — | 20/16 | Previtelliform | OS | OS | OS |
| S9 | F7 | 63 | F | *IMPG2* | OD | 20/40 | Atrophic with CNV | OD | OD | OD |
| | | | | | OS | 20/32 | Atrophic | OS | OS | OS |
| S10 | F8 | 37 | F | Inconclusive | OD | 20/32 | Atrophic with CNV | — | OD | OD |
| | | | | | OS | 20/50 | Atrophic with CNV | OS | OS | OS |
| S11 | F9 | 48 | M | Inconclusive | OD | 20/20 | Vitelliform, Multifocal | OD | OD | OD |
| | | | | | OS | 20/25 | Vitelliform, Multifocal | — | OS | OS |

BCVA, best-corrected visual acuity; CNV, choroidal neovascularization.

[*] S8 is the father of S7; S2 and S3 are twin monozygotic brothers.

[†] Family number.

[‡] Five patients had vitelliform lesions in one eye only; "—" denotes no vitelliform lesion present at the time of evaluation.

[§] S9: CNV stable, s/p bevacizumab.

[‖] Longitudinal imaging was performed in four patients (months in between follow up visits are indicated in the parenthesis). "—" denotes that AO imaging was not performed in that eye. S8 declined ICG injection; only cone photoreceptor imaging was performed.

[#] FfERG and EOG were recorded in a subset of patients. "—" denotes that the test was not performed in that eye.

[**] S2: only clinical imaging was performed at the follow-up visit (not AO).

surrounding the lesion. Within each RPE ROI, a smaller cone ROI was selected. If a subject did not undergo ICG, then only cone ROIs were selected in the juxtalesional area. For the nonlesion ROIs outside of the juxtalesional area, to account for the rapid change in cone density at smaller eccentricities, ROIs were selected at smaller intervals of 0.1 mm at eccentricities smaller than 1.0 mm and larger intervals of 1.0 mm at eccentricities larger than 1.5 mm. The smallest eccentricity at which these non-lesion cone ROIs could be selected was limited by the varying size of the macular lesions. For contralateral eyes of five subjects with macular lesions in only one eye (Table), ROIs within 2.5 mm of the lesion edge were selected at symmetrically matching locations (mirror image), with minor adjustments to avoid blood vessels present at the mirror location in the contralateral eye.

Individual cells were sequentially marked by three expert graders. The first grader applied machine learning-based algorithms for automated identification of cone[36] and RPE cells[37] and performed manual adjustments to automatically detected cells when necessary. The second expert grader performed further manual correction before final verification by a third expert grader. Disagreements in cell identification were addressed through a reconciliation process involving additional iterative manual correction of the images between two of the graders until either full agreement was reached or the image was discarded. These cell centers were then used to generate Voronoi diagrams from which cell densities were calculated. Any Voronoi neighborhood that exceeded the boundary of the ROI was discarded, with the number of remaining cells divided by the total area of the corresponding Voronoi neighborhoods remaining (examples of RPE annotation, based on the assumption that individual RPE cells have uniform fluorescence[29,30,38] are shown in Supplementary Fig. S1). The PRL was determined as the average centroid from image sequences during which the subject was asked to look at the center of the field of view. The location of this PRL was compared with the center of the foveal pit as imaged using OCT, to verify whether the PRL coincided with the anatomical fovea. If the PRL did not coincide with the anatomical fovea (e.g., due to macular atrophy or the presence of a lesion), then the anatomical fovea was used to determine the retinal eccentricity for each ROI; otherwise, the PRL was used. In addition, the edge of the macular lesion was manually identified based on AO imaging (also confirmed to be consistent with co-registered clinical imaging including color fundus photography, OCT, and for a subset of patients, autofluorescence). The coordinates of each ROI were also plotted as a function of distance from the lesion based on the length of the shortest line between the ROI centroid and the nearest lesion edge. The retinal magnification factor to scale image distances from degrees to millimeters were computed based on ocular biometry measurements acquired after dilation (axial length, corneal curvature, and anterior chamber depth) (IOL Master; Carl Zeiss Meditec, Dublin, CA, USA), as previously described.[39]

Investigative Ophthalmology & Visual Science

Downloaded from hwmaint.iovs.org on 04/24/2024

### Statistical Analysis

The statistical analysis was performed using a one-way analysis of variance (ANOVA) followed by Bonferroni's test for six pairwise comparisons between each pair of genes (e.g., *IMPG1* vs. *IMPG2*, *IMPG1* vs. *PRPH2*, *IMPG1* vs. *BEST1*, etc.), with a significance value of 0.05. For the comparisons across genes in affected eyes, for patients who had both eyes imaged, only the right eye was selected for the comparison of cone and RPE measurements; otherwise, if only one eye was imaged, then that eye was included (N = 11 eyes from 11 patients).

## Results

### Clinical Assessment

Eleven subjects from nine families with VMD due to genetic etiology were included in this study: four females, seven males with a mean age of 39.8 years (range 17–65). The stage of vitelliform lesion ranged from stage 1 (previtelliform) to stage 5 (atrophic) (Table). Six patients had bilateral disease whereas five patients were noted to have no vitelliform macular lesion or near-normal maculae (previtelliform) in one eye and were considered to be "non-lesion" eyes (n = 5) for the purposes of this study. Five eyes of three patients had multifocal disease with multiple vitelliform lesions in the posterior pole. Seven patients completed ERG and of these, six patients had normal scotopic function such that EOG Arden ratio could be interpreted (Table). Mean Arden ratio for the *BEST1* group was 1.4 (n = 2 eyes), *IMPG1* 2.1 (n = 2 eyes), *IMPG2* 3.1 (n = 2 eyes), *PRPH2* 2.0 (n = 3 eyes), and in the patient with inconclusive genetic testing results (subject S11), 3.3 (n = 2 eyes). Molecular diagnostic testing revealed causative, pathogenic variants in *BEST1, PRPH2, IMPG1,* or *IMPG2* in nine patients; a molecular cause could not be identified in two patients.

### Cone and RPE Density in Lesion Areas

Multimodal AO imaging in eyes with VMD resulting from mutations in *BEST1*, *PRPH2, IMPG1,* and *IMPG2* provided cellular level resolution to visualize both cones and RPE cells (Fig. 1). Within the lesional areas, anteriorly displaced photoreceptors located above the macular lesions were

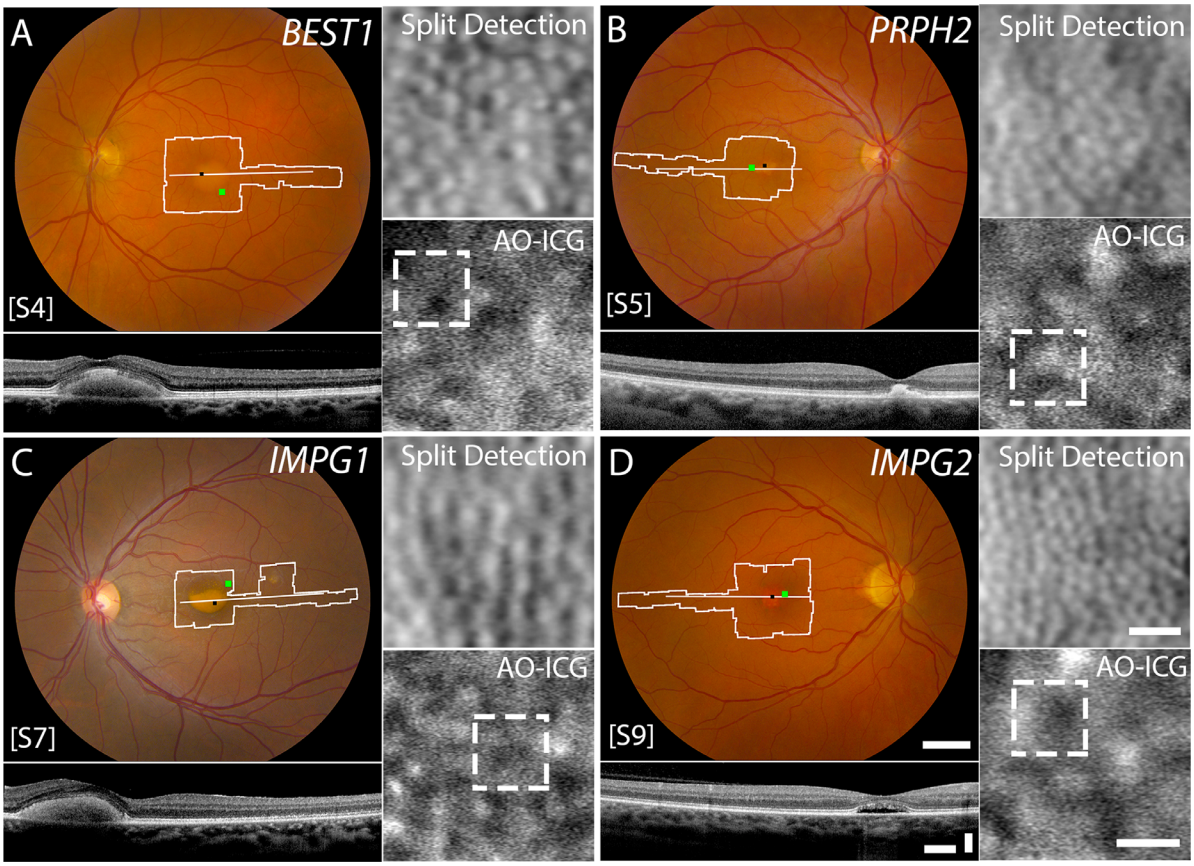


**Figure 1.** Multimodal AO imaging in eyes with VMD resulting from mutations in (**A**) *BEST1*, (**B**) *PRPH2*, (**C**) *IMPG1*, and (**D**) *IMPG2*. The color fundus photographs show a single macular lesion except for subject S7 who has a second smaller lesion temporal to the central lesion [subject codes given in brackets]. OCT shows elevated photoreceptors corresponding to the central macular lesions. Both cone photoreceptors and RPE cells appear structurally intact imaged using non-confocal split detection[28] and late-phase AO-ICG imaging,[29,30] respectively. Individual RPE cells can be distinguished by the heterogeneous cyanescent pattern.[37] Superimposed on the color fundus: *irregularly-shaped white outlines* indicating locations where overlapping AO images were acquired in each eye, *horizontal line* corresponding to the OCT b-scan, and a *small black square* indicating the foveal center (eccentricity = 0.0 mm, determined based on the subject's preferred retinal locus of fixation as imaged using AO). The *small green square* indicates the location corresponding to the AO-ICG image of the RPE shown to the right of each color fundus, and the *dashed white square* in the AO-ICG images indicates the location corresponding to the non-confocal split detection image of cones. *Scale bars*: color fundus, 2 mm; OCT, 500 µm (horizontal), 200 µm (vertical); AO-ICG, 50 µm; Split Detection, 15 µm.

Investigative Ophthalmology & Visual Science

Downloaded from hwmaint.iovs.org on 04/24/2024

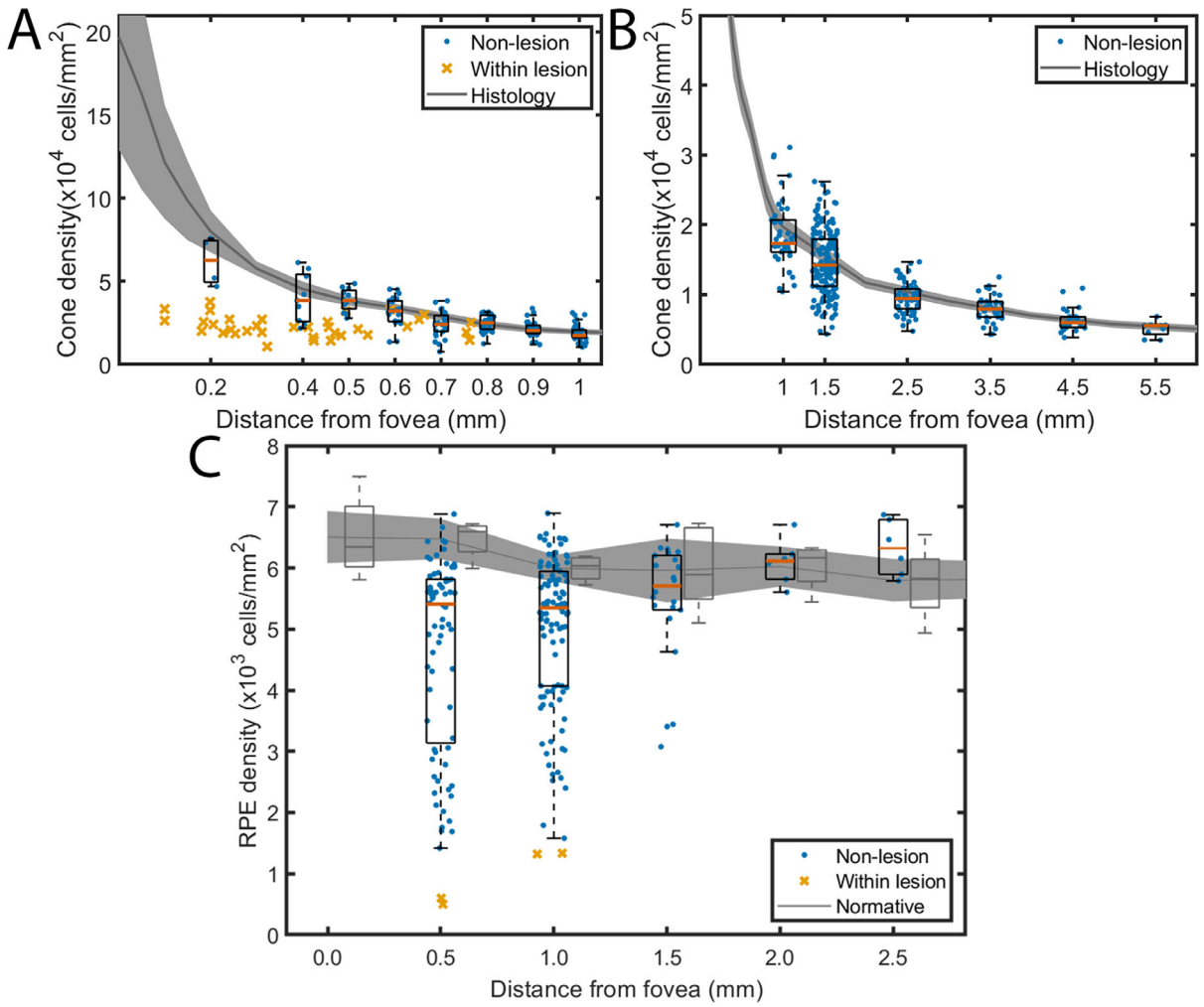


**Figure 2.** Cone and RPE density measurements performed using multimodal AO imaging in eyes with VMD, plotted as boxplots with individual datapoints overlaid. For visualization purposes, the median of each boxplot is vermillion colored. (**A, B**) Cones density measured outside of macular lesions (*blue*) straddled normative data[40] at most eccentricities. However, cone density measured above lesions (*orange*) were reduced below normal values. The cone density plot was split at the 1 mm eccentricity. At the eccentricities closer to the fovea (≤1 mm, panel **A**), additional measurements of cone density were performed to account for the sharp increase in cone density in this region. The gray band represents the 95% confidence interval around the average normal cone density (*gray line*). (**C**) RPE density measured outside of macular lesions (*blue*) were highly variable at locations closer to the fovea (0.5 and 1.0 mm) but were similar to normative data[41] further from the fovea (1.5-2.5 mm). RPE density measurements performed within lesions (*orange*) were substantially reduced. The *gray band* represents the 95% confidence interval around the average normal RPE density (*gray line*).

visible in 14 out of 15 eyes, including some cones with abnormal cellular morphology (i.e., not circular in shape) (Supplementary Fig. S2), as has been previously described in Best VMD.[27] Cone densities measured above the macular lesions were reduced well below normal values,[40] to 37% of normal cone density at an eccentricity of 0.2 mm (only ROIs containing circular cone morphologies were quantified). Unfortunately, RPE cells could not be successfully visualized beneath lesions due to blocking of the late phase ICG signal by the vitelliform material, aside from a few select locations where the vitelliform material had resorbed (two of 15 eyes) (Supplementary Fig. S3). In these select locations, RPE density was substantially reduced, well below normal values,[41] to 8.4% of normal RPE density at an eccentricity of 0.5 mm. Due to the relatively few areas where RPE could be visualized within lesional areas, we restricted most of our analysis in the subsequent sections comparing cones and RPE to non-lesion areas of the eyes.

## Cone and RPE Density Outside of Lesion Areas

In all 15 eyes with macular lesions associated with VMD, structurally intact cone photoreceptors were observed across the retina in non-lesion areas out to 5.5 mm eccentricity in the temporal direction. Quantification of 473 distinct cone regions of interest (ROIs) revealed that on average, the cones were similar to expected histologic normative values at most eccentricities[40] (Figs. 2A, 2B). Averaged across the eccentricities (0.2 to 5.5 mm), cone density was slightly reduced to 90% of the normal value. However, there was considerable variability at eccentricities <1 mm (Fig. 2A), with the greatest decrease in cone density observed at 0.2 mm eccentricity (76% of the normal value), possibly due to the close proximity to macular lesions.

Likewise, in all eyes, RPE cells were intact across the retina in non-lesion areas out to 2.5 mm eccentricity in the temporal direction, and exhibited the characteristic

Investigative Ophthalmology & Visual Science

Downloaded from hwmaint.iovs.org on 04/24/2024

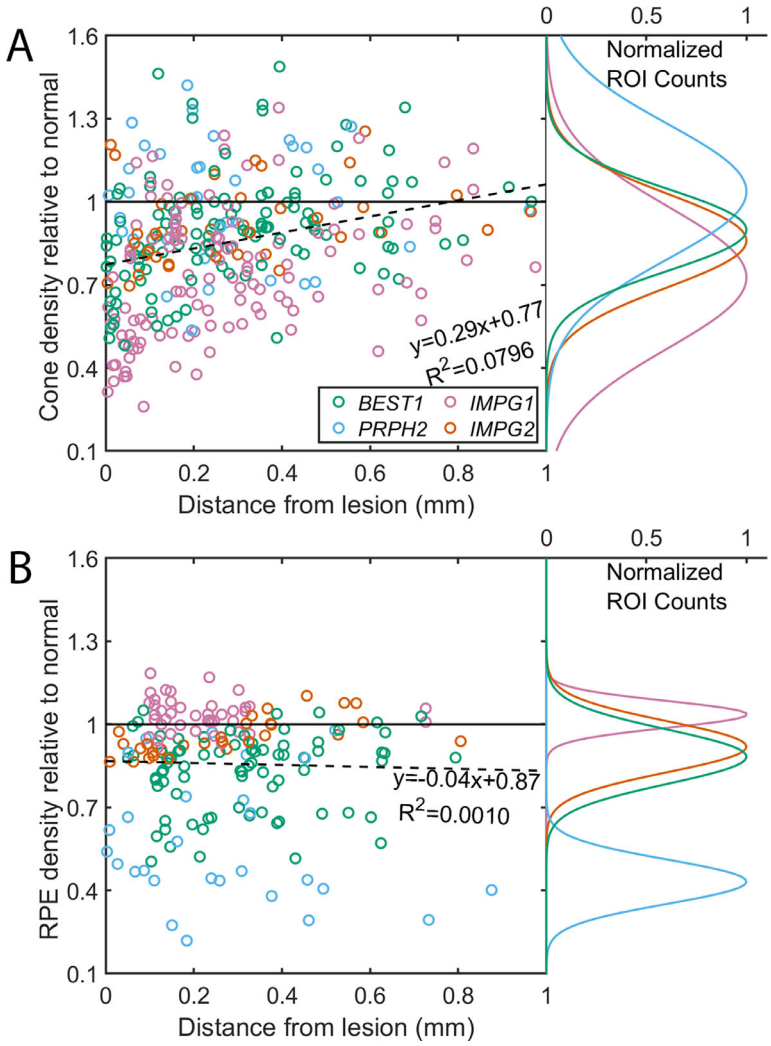


**Figure 3.** Normalized cone and RPE density in juxtalesional areas < 1 mm from the edge of the lesion, replotted according to distance from lesion, and categorized according to gene. Normalized gaussian fits are shown to the right of each plot. (**A**) Cone density was most decreased in *IMPG1*, followed by *IMPG2*, *BEST1*, and *PRPH2*. (**B**) RPE density was most decreased in *PRPH2,* followed by *BEST1, IMPG2,* and *IMPG1*, the opposite order as **A**.

heterogeneous pattern of fluorescence we previously reported in normal and diseased eyes[29,30] (Fig. 2C). Quantification of 213 distinct RPE ROIs revealed slightly decreased RPE density compared to normative values,[41] albeit with considerable variation in the individual measurements (Fig. 2C). For example, at 0.5 mm eccentricity, the smallest non-lesion RPE density measured was 22% of the normal value. Nonetheless, on average, across the eccentricities (0.5 to 2.5 mm), RPE density was only slightly reduced, also to 92% of the normal value.

## Juxtalesional Cone and RPE Density

To better reveal the status of juxtalesional cells, measurements of cone and RPE density were replotted as a function of distance from the edge of the macular lesion and ROIs located within 1 mm of the edge were considered. Given the variation in size of macular lesions from eye to eye, cone and RPE densities were normalized to the expected normative value at the eccentricity corresponding to each ROI (e.g., a normalized value <1 indicates a reduction in density relative to normal). In general, for both cones and RPE cells in this juxtalesional area (<1 mm from the lesion edges), there was no apparent relationship between distance from the lesion and cell density (Fig. 3). The absence of a gradual increase or decrease in density as the lesion is approached (i.e., as the distance goes to 0) suggests the absence of a transition zone surrounding the lesion. However, it is likely that there is a transition zone for cones within the vitelliform lesion between abnormal and normal cone density (Supplementary Fig. S4).

## Classification of Cone and RPE Density According to Gene

Further classification of normalized RPE density according to gene revealed differences between genes in this patient cohort. In particular, the greatest decrease in RPE density was observed in *PRPH2*, followed by *BEST1, IMPG2,* and *IMPG1* (the average RPE density for *IMPG1* was supranormal) (Fig. 3B). There were statistically significant differences

Investigative Ophthalmology & Visual Science

Downloaded from hwmaint.iovs.org on 04/24/2024

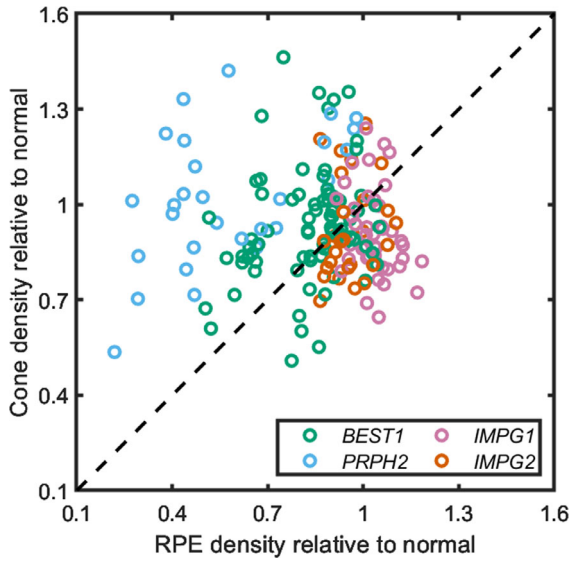


Figure 4. Relationship between cone and RPE density measurements performed at juxtalesional regions within 1 mm from the edge of the lesion, grouped by gene. The 1:1 *dashed line* indicates equal disruption to both cones and RPE; points to the left of the line indicate greater RPE disruption compared to cone disruption; points to the right indicate greater cone disruption compared to RPE disruption.

in RPE density between all pairwise comparisons performed between genes (Bonferroni corrected $P < 0.05$ for all pairwise comparison). Although there was increased variability in cone density in this same region, the degree to which cones were affected relative to the genes followed the inverse order with the greatest decreases in cone density observed in *IMPG1,* followed by *IMPG2, BEST1,* and then *PRPH2* (the average cone density for *PRPH2* was supranormal) (Fig. 3A). There were statistically significant differences in cone density between *IMPG1* and each of the other three genes (Bonferroni corrected $P < 0.05$). There were no significant differences in cone density observed between *BEST1* and *IMPG2* ($P = 0.12$, Bonferroni corrected $P = 0.75$), *BEST1* and *PRPH2* ($P = 0.45$, Bonferroni corrected $P = 2.73$), or *PRPH2* and *IMPG2* ($P = 0.57$, Bonferroni corrected $P = 3.44$). These trends appeared to hold across the entire range of distances up to 1 mm from the edge of the lesion, especially for the RPE (e.g., RPE density in *PRPH2* was consistently lower than those of other genes between 0 to 1 mm from the edge of the lesion).

The capability to assess both cone photoreceptors and RPE cells at the same retinal location within the living human eye provided an opportunity to examine cone-RPE relationships with respect to the different genes. To explore these relationships, the juxtalesional cone and RPE cell densities (<1 mm from the lesion edge) were plotted against each other (Fig. 4). Here, the 1:1 dashed line indicates equal disruption to both the cones and RPE cells; points to the left of this line indicate greater RPE than cone disruption, and points to the right indicate greater cone than RPE disruption. The data shows that 73% of the ROIs from patients with *IMPG1* and *IMPG2* mutations were below the dashed line, suggesting that overall, cone photoreceptors were more affected than RPE cells in patients harboring mutations in these genes. Conversely, 100% of the ROIs from patients with *PRPH2* mutations and 69% of the ROIs from patients with *BEST1* mutations were above the dashed line, suggesting that, in general, RPE cells were more affected than cones in patients harboring mutations in these genes. The data points associated with *PRPH2* mutations were scattered to a greater extent to the left of the dashed line, indicating more severe damage to the RPE compared to *BEST1*.

## Evaluation of Cone and RPE Density in Unilateral VMD

Thus far, our analysis considered only juxtalesional areas within eyes with macular lesions associated with VMD. Next, we further explored whether mutations in these genes could impact the contralateral eyes of five subjects with macular lesions in only one eye (Table). These contralateral eyes were relatively unaffected compared to the affected eyes, and as expected AO images acquired in these eyes revealed structurally intact cone photoreceptors and RPE cells throughout the imaged areas (Figs. 5 and 6). Qualitative comparison of pairs of cone and RPE ROIs acquired at symmetric locations in both eyes revealed no qualitative differences in cone or RPE structure.

Further quantification on 126 pairs of cone ROIs and 53 pairs of RPE ROIs at symmetrically matching locations (mirror image) also revealed differences in relative cone and RPE density across the genes. For this analysis, a slightly larger juxtalesional area was selected (2.5 mm from the lesion edge) to allow for positions of ROIs in the non-lesion eyes to be slightly adjusted to avoid arterioles and venules (Fig. 7). Although intraocular symmetry might be expected for normal cone density measurements,[42] it was surprising that abnormal (reduced) cone and RPE densities were symmetrically observed in the relatively unaffected non-lesion eyes, especially for the RPE (indicated by data points clustering around the 1:1 dashed line). These data provide evidence that the retinal areas thought to be affected by pathogenic mutations may extend further than areas where clinically evident lesions are observed. In this subset patients, ROIs associated with *IMPG1* were found to cluster together at lower cone densities relative to those from *BEST1*, further corroborating our earlier finding that *IMPG1* has a greater effect on cones than RPE cells. This phenomenon was reversed in the RPE plot, indicating that *BEST1* affects the RPE to a greater extent than the cones.

## Assessment of Cone and RPE Density in Areas of Lesion Expansion or Resorption

Finally, we examined longitudinal images from five eyes to assess changes at the cellular level due to expansion or resorption of the macular lesion. In particular, 21 ROIs for cones and 18 ROIs for RPE were identified in areas where intact cones and RPE were present in one visit but subsequently covered by an expanding vitelliform lesion at a follow-up visit (pre-expansion ROIs). Conversely, seven ROIs for cones and eight ROIs for RPE were identified in areas that were previously covered but were revealed because of resorption of the vitelliform material in a subsequent visit (resorption ROIs). In general, cone and RPE density was only slightly reduced before expansion of the vitelliform lesion; after resorption of the vitelliform material, both cone and RPE density were further reduced, with the greatest reduction occurring in the RPE (Fig. 8). However,

Investigative Ophthalmology & Visual Science

Downloaded from hwmaint.iovs.org on 04/24/2024

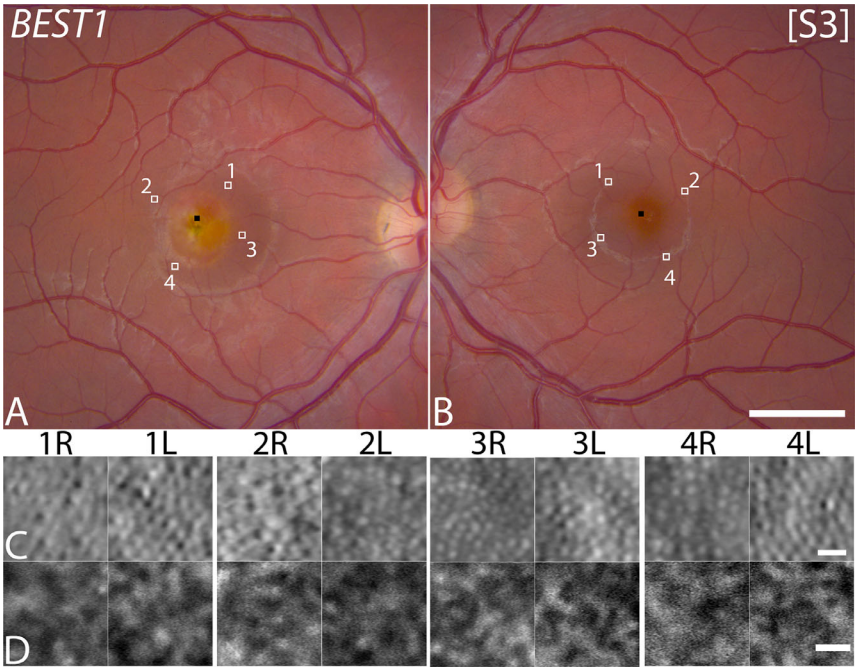


**Figure 5.** Comparison of AO imaging in matched symmetric locations across contralateral eyes of a patient with a macular lesion associated with *BEST1* VMD in only one eye. (**A, B**) Color fundus photographs. The small black square indicates the foveal center (eccentricity = 0.0 mm, determined based on the subject's preferred retinal locus of fixation as imaged using AO. Numbered small white squares indicate locations of stacked ROIs showing (**C**) cone photoreceptors imaged using non-confocal split detection taken from within a larger ROI of (**D**) RPE cells imaged using AO-ICG. The eccentricity dependent variation in cell size is much more apparent for cones than RPE (see normative data in Fig. 2). *Scale bars*: color fundus, 2 mm; **C**, 15 µm; **D**, 50 µm.

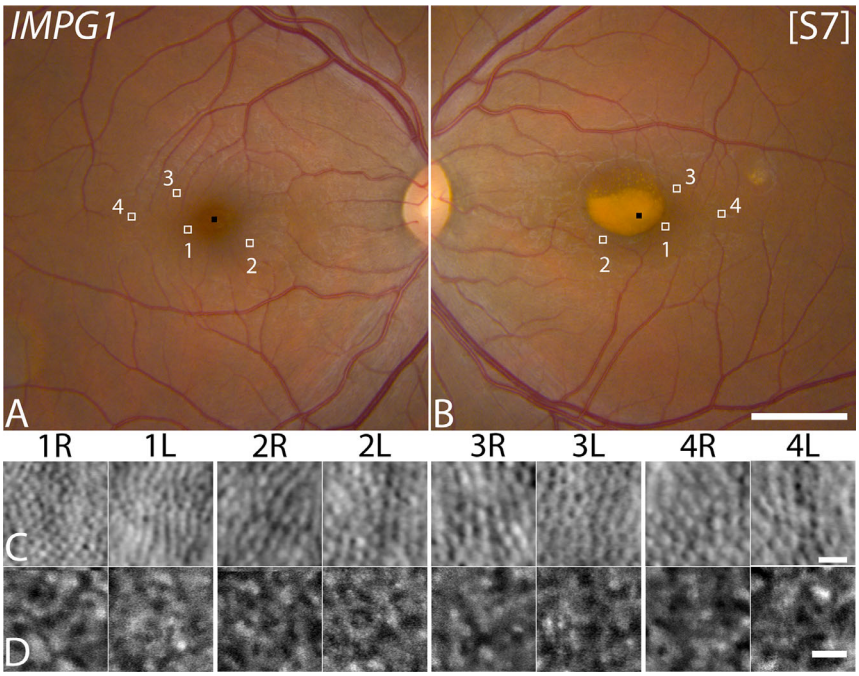


**Figure 6.** Comparison of AO imaging in matched symmetric locations across contralateral eyes of a patient with a macular lesion associated with *IMPG1* VMD in only one eye. (**A, B**) Color fundus photographs. The *small black square* indicates the foveal center (eccentricity = 0.0 mm, determined based on the subject's preferred retinal locus of fixation as imaged using AO. *Numbered small white squares* indicate locations of stacked ROIs showing (**C**) cone photoreceptors imaged using non-confocal split detection taken from within a larger ROI of (**D**) RPE cells imaged using AO-ICG. The eccentricity-dependent variation in cell size is much more apparent for cones than RPE (see normative data in Fig. 2). *Scale bars*: color fundus, 2 mm; **C**, 15 µm; **D**, 50 µm.

Investigative Ophthalmology & Visual Science

Downloaded from hwmaint.iovs.org on 04/24/2024

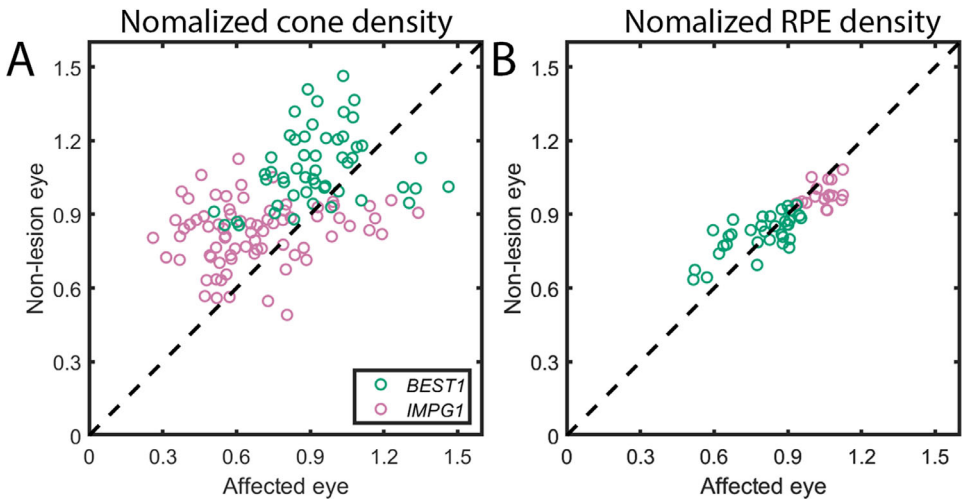


**Figure 7.** Comparison of cone and RPE density measurements performed at symmetrically matching locations between contralateral eyes in patients with VMD who had macular lesions in only one eye. Measurements were performed at locations corresponding to within 2.5 mm juxtalesional to the macular lesion of the affected eye. (**A**) Normalized cone density measurements performed in two patients with *IMPG1* VMD and three patients with *BEST1* VMD. (**B**) Normalized RPE density measurements performed in one patient with *IMPG1* VMD and three patients with *BEST1* VMD (subject S8 declined ICG; see Table). The clustering of points around the 1:1 line in the RPE plot indicates symmetric RPE disruption between contralateral eyes of these patients.

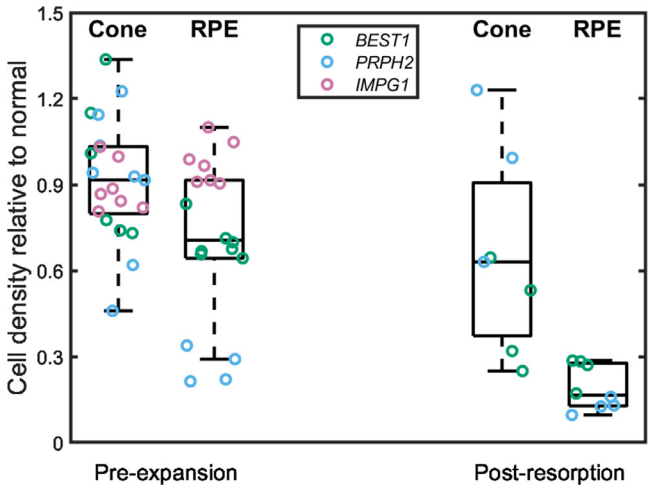


**Figure 8.** Assessment of cones and RPE imaged in areas before expansion and after resorption of the vitelliform material. Normalized cone and RPE density measurements acquired from the patients were plotted as boxplots with individual datapoints overlaid. In non-lesion areas before expansion, RPE density was reduced to a greater extent in *PRPH2* and *BEST1* compared to *IMPG1*. After resorption, RPE density was decreased for both *PRPH2 and BEST1*. No resorption was observed in the patients with *IMPG1* VMD.

as we have shown in this article, it is important to take into consideration the underlying genetic etiology. When categorized according to gene, stratification of the RPE density measurements is evident with the lowest baseline RPE density measurements observed in *PRPH2,* followed by *BEST1* (near normal RPE density was observed in *IMPG1*). For both *PRPH2* and *BEST1*, a further reduction in RPE density was still observed after resorption. Generally, cones appeared to be less affected after resorption for both *PRPH2* and *BEST1*. These preliminary findings may be useful for informing future studies.

## Discussion

Quantitative assessment of cone photoreceptors and RPE cell mosaics revealed that differences in cell density were stratified across different genes associated with VMD (Fig. 4). Our cone density measurements are in good agreement with a previous study measuring cones above and outside of vitelliform lesions[27] but extend these to a broader cohort of patients with VMD attributed to other genes and provide the first in vivo measurements of RPE density, to our knowledge, in VMD. Surprisingly, differences in cone and RPE density across genes not only were observed in the juxtalesional (<1 mm) areas surrounding macular lesions but also were symmetrically observed in contralateral eyes of five patients without any identifiable vitelliform lesions (Fig. 7). It should be noted that these decreases in both cone and RPE density occurred within intact cone and RPE mosaics, which would not be expected to be detectable using conventional imaging approaches such as fundus autofluorescence or OCT, which have been examined in previous studies.[43] These subclinical quantitative AO measurements demonstrate a possible strategy for examining genotype-phenotype relationships and may be useful for assisting with the interpretation of eyes with VMD but inconclusive genetic testing results.

Whereas the majority of patients in this study had a variant in a gene known to cause VMD (Supplementary Table S1), two patients had inconclusive results. Subject S10 had two variants, including a frameshift mutation in the *IMPG1* gene that was classified as likely pathogenic according to ACMG criteria. Intriguingly, this subject had relative cone/RPE densities indicative of greater cone disruption than RPE, with points clustered near those of *IMPG1* (circles, Fig. 9 and Supplementary Fig. S5). However, this variant was inherited from the paternal side, with the father reporting normal eye exams and negative family history. Of interest, this patient has a strong family history of VMD on the maternal side with an affected mother and maternal grandmother. All three affected individuals shared a missense variant of unknown significance in the *PRPF31*.

Investigative Ophthalmology & Visual Science

Downloaded from hwmaint.iovs.org on 04/24/2024

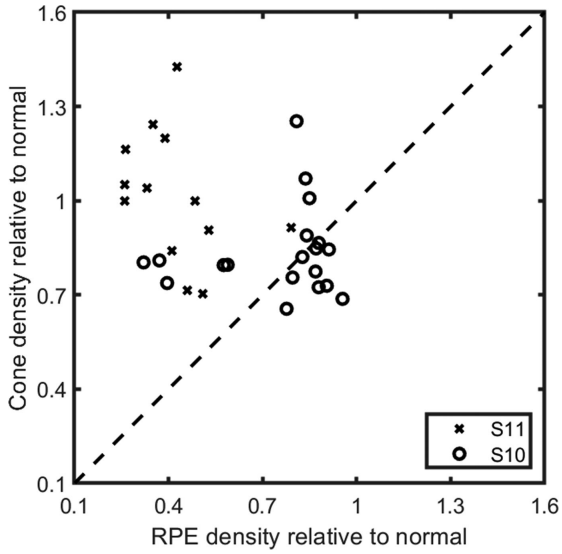


**Figure 9.** Relationship between cone and RPE density measurements performed at juxtalesional regions within 1 mm from the edge of the lesion in two patients with inconclusive genetic testing results (see Fig. 4). The datapoints from S11 are to the left of the 1:1 line, indicating that S11 has greater RPE disruption relative to cone disruption.

*PRPF31* has not been previously reported in association with VMD. Subject S11 had no identified causative variants and was reported as having indeterminate results on a gene panel for hereditary retinopathies. The relative cone/RPE densities were indicative of greater RPE disruption than cone, with points that clustered near those of *PRPH2* (crosses, Fig. 9 and Supplementary Fig. S5).

In a subset of patients who had both ffERG (including 30 Hz cone flicker) and EOG performed, relationships between 30 Hz cone flicker amplitudes (related to cone function) and Arden ratio (related to RPE function in patients with normal scotopic ffERGs) (Supplementary Fig. S6) mirrored the comparison plot between cone and RPE density (Fig. 4). In particular, the patients with *IMPG1* and *IMPG2* mutations have relatively lower cone function in comparison to RPE function; in contrast, patients with *BEST1* and *PRPH2* have relatively lower RPE function in comparison to cone function. The consistent reduction in RPE function observed in *PRPH2* (Fig. 4 and Supplementary Fig. S6) is intriguing because this gene encodes a protein located in the photoreceptor outer segments. It should be noted that whereas the AO cell density measurements were performed only at select ROIs in non-lesion portions of the retina (outside of the lesion), the ffERG and EOG measurements reflect a global retinal response, covering both the vitelliform and non-vitelliform regions of the retina. In addition, ffERG and EOG are not pure measurements of cone and RPE function. Nonetheless, the similarity in trend observed is indicative of a structure function relationship between AO and ffERG/EOG data.

We acknowledge that an inherent limitation of this study is that the number of patients (N = 11) is relatively small, and additional patients are needed to further explore these findings. Nevertheless, to our knowledge, this is the largest dataset examining cones and RPE in VMD using AO. Across the 20 eyes imaged, over 700 ROIs containing over 62,000 cells were quantified for analysis.

In conclusion, multimodal AO imaging using both nonconfocal split detection and AO-ICG provides a way to simultaneously assess the cone photoreceptors and the RPE in eyes with VMD. Monitoring RPE status in juxtalesional areas outside of the macular lesions as well as in contralateral eyes without visible vitelliform lesions may be particularly important in patients with VMD associated with *PRPH2*- and *BEST1*; likewise, monitoring cone status may be important in patients with VMD associated with *IMPG1* and *IMPG2*. Our findings provide new insights into the gene-dependent mechanisms of disease in VMD.

## Acknowledgments

The authors thank HaeWon Jung and Rongwen Lu for assistance with adaptive optics imaging, Jianfei Liu and Andrei Volkov for assistance with adaptive optics image processing software, Angel Garced, Daniel Claus, Allison Bamji, and Wendy Holland for assistance with patient coordination; Gloria Babilonia-Ayukawa, Mike Arango, Denise Cunningham, Christina Appleman, Sharon Yin, Jenny Suy, John Rowan, and Guy Foster for assistance with clinical procedures.

Supported by the Intramural Research Program of the National Institutes of Health, National Eye Institute, the Alcon Research Institute, Research to Prevent Blindness (Departmental award) and National Eye Institute awards P30EY026877, R01EY031360, R01EY032147 and R01EY032669. This content is solely the responsibility of the authors and does not necessarily represent the official views of the National Institutes of Health. The mention of commercial products, their sources, or their use in connection with material reported herein is not to be construed as either an actual or implied endorsement of such products by the U.S. Department of Health and Human Services.

Disclosure: **T. Liu,** None; **N. Aguilera,** None; **A.J. Bower,** None; **J. Li,** None; **E. Ullah,** None; **A. Dubra,** None; **C. Cukras,** None; **B.P. Brooks,** None; **B.G. Jeffrey,** None; **R.B. Hufnagel,** None; **L.A. Huryn,** None; **W.M. Zein,** None; **J. Tam,** None

## References

1. Dalvin LA, Pulido JS, Marmorstein AD. Vitelliform dystrophies: prevalence in Olmsted County, Minnesota, United States. *Ophthalmic Genet*. 2017;38:143–147.
2. Mohler CW, Fine SL. Long-term evaluation of patients with Best's vitelliform dystrophy. *Ophthalmology*. 1981;88:688–692.
3. Querques G, Zerbib J, Georges A, et al. Multimodal analysis of the progression of Best vitelliform macular dystrophy. *Mol Vision*. 2014;20:575–592.
4. Johnson AA, Guziewicz KE, Lee CJ, et al. Bestrophin 1 and retinal disease. *Prog Retinal Eye Res*. 2017;58:45–69.
5. Meunier I, Sénéchal A, Dhaenens C-M, et al. Systematic screening of BEST1 and PRPH2 in juvenile and adult vitelliform macular dystrophies: a rationale for molecular analysis. *Ophthalmology*. 2011;118:1130–1136.
6. Querques G, Forte R, Querques L, Massamba N, Souied EH. Natural course of adult-onset foveomacular vitelliform dystrophy: a spectral-domain optical coherence tomography analysis. *Am J Ophthalmol*. 2011;152:304–313.
7. Tiosano L, Grunin M, Hagbi-Levi S, Banin E, Averbukh E, Chowers I. Characterising the phenotype and progression of sporadic adult-onset foveomacular vitelliform dystrophy. *Br J Ophthalmol*. 2016;100:1476–1481.
8. Arora R, Khan K, Kasilian ML, et al. Unilateral BEST1-associated retinopathy. *Am J Ophthalmol*. 2016;169:24–32.



Downloaded from hwmaint.iovs.org on 04/24/2024

9. Boon CJ, Klevering BJ, den Hollander AI, et al. Clinical and genetic heterogeneity in multifocal vitelliform dystrophy. *Arch Ophthalmol*. 2007;125:1100–1106.
10. Marmorstein AD, Marmorstein LY, Rayborn M, Wang X, Hollyfield JG, Petrukhin K. Bestrophin, the product of the Best vitelliform macular dystrophy gene (VMD2), localizes to the basolateral plasma membrane of the retinal pigment epithelium. *Proc Natl Acad Sci*. 2000;97:12758–12763.
11. Singh R, Shen W, Kuai D, et al. iPS cell modeling of Best disease: insights into the pathophysiology of an inherited macular degeneration. *Hum Mol Genet*. 2013;22:593–607.
12. Marmorstein AD, Kinnick TR, Stanton JB, Johnson AA, Lynch RM, Marmorstein LY. Bestrophin-1 influences transepithelial electrical properties and Ca2+ signaling in human retinal pigment epithelium. *Mol Vision*. 2015;21:347–359.
13. Petrukhin K, Koisti MJ, Bakall B, et al. Identification of the gene responsible for Best macular dystrophy. *Nat Genet*. 1998;19:241–247.
14. Marquardt A, Stöhr H, Passmore LA, Krämer F, Rivera A, Weber BH. Mutations in a novel gene, VMD2; encoding a protein of unknown properties cause juvenile-onset vitelliform macular dystrophy (best's disease). *Hum Mol Genet*. 1998;7:1517–1525.
15. Guziewicz KE, Sinha D, Gómez NM, et al. Bestrophinopathy: an RPE-photoreceptor interface disease. *Progr Retinal Eye Res*. 2017;58:70–88.
16. Frangieh GT, Green WR, Fine SL. A histopathologic study of Best's macular dystrophy. *Arch Ophthalmol*. 1982;100:1115–1121.
17. Mullins RF, Kuehn MH, Faidley EA, Syed NA, Stone EM. Differential macular and peripheral expression of bestrophin in human eyes and its implication for best disease. *Invest Ophthalmol Vis Sci*. 2007;48:3372–3380.
18. Boon CJ, den Hollander AI, Hoyng CB, Cremers FP, Klevering BJ, Keunen JE. The spectrum of retinal dystrophies caused by mutations in the peripherin/RDS gene. *Progr Retinal Eye Res*. 2008;27:213–235.
19. Reeves MJ, Goetz KE, Guan B, et al. Genotype–phenotype associations in a large PRPH2-related retinopathy cohort. *Hum Mutat*. 2020;41:1528–1539.
20. Meunier I, Manes G, Bocquet B, et al. Frequency and clinical pattern of vitelliform macular dystrophy caused by mutations of interphotoreceptor matrix IMPG1 and IMPG2 genes. *Ophthalmology*. 2014;121:2406–2414.
21. Poetsch A, Molday LL, Molday RS. The cGMP-gated channel and related glutamic acid-rich proteins interact with peripherin-2 at the rim region of rod photoreceptor disc membranes. *J Biol Chem*. 2001;276:48009–48016.
22. Chakraborty D, Conley SM, Stuck MW, Naash MI. Differences in RDS trafficking, assembly and function in cones versus rods: insights from studies of C150S-RDS. *Hum Mol Genet*. 2010;19:4799–4812.
23. Salido EM, Ramamurthy V. Proteoglycan IMPG2 shapes the interphotoreceptor matrix and modulates vision. *J Neurosci*. 2020;40:4059–4072.
24. Roorda A, Duncan JL. Adaptive optics ophthalmoscopy. *Ann Rev Vis Sci*. 2015;1:19–50.
25. Duncan JL, Zhang Y, Gandhi J, et al. High-resolution imaging with adaptive optics in patients with inherited retinal degeneration. *Invest Ophthalmol Vis Sci*. 2007;48:3283–3291.
26. Kay DB, Land ME, Cooper RF, et al. Outer retinal structure in best vitelliform macular dystrophy. *JAMA Ophthalmol*. 2013;131:1207–1215.
27. Scoles D, Sulai YN, Cooper RF, et al. Photoreceptor inner segment morphology in best vitelliform macular dystrophy. *Retina*. 2017;37:741–748.
28. Scoles D, Sulai YN, Langlo CS, et al. In vivo imaging of human cone photoreceptor inner segments. *Invest Ophthalmol Vis Sci*. 2014;55:4244–4251.
29. Tam J, Liu J, Dubra A, Fariss R. In vivo imaging of the human retinal pigment epithelial mosaic using adaptive optics enhanced indocyanine green ophthalmoscopy. *Invest Ophthalmol Vis Sci*. 2016;57:4376–4384.
30. Jung H, Liu J, Liu T, et al. Longitudinal adaptive optics fluorescence microscopy reveals cellular mosaicism in patients. *JCI Insight*. 2019;4(6):e124904.
31. McCulloch DL, Marmor MF, Brigell MG, et al. ISCEV Standard for full-field clinical electroretinography (2015 update). *Doc Ophthalmol*. 2015;130:1–12.
32. Constable PA, Bach M, Frishman LJ, Jeffrey BG, Robson AG. ISCEV Standard for clinical electro-oculography (2017 update). *Doc Ophthalmol*. 2017;134:1–9.
33. Thavikulwat AT, Lopez P, Caruso RC, Jeffrey BG. The effects of gender and age on the range of the normal human electro-oculogram. *Doc Ophthalmol*. 2015;131:177–188.
34. Dubra A, Harvey Z. Registration of 2D images from fast scanning ophthalmic instruments. In: Fischer B, Dawant BM, Lorenz C , eds. *International Workshop on Biomedical Image Registration*. Berlin: Springer; 2010:60–71.
35. Cooper RF, Wilk MA, Tarima S, Carroll J. Evaluating descriptive metrics of the human cone mosaic. *Invest Ophthalmol Vis Sci*. 2016;57:2992–3001.
36. Liu J, Shen C, Aguilera N, et al. Active cell appearance model induced generative adversarial networks for annotation-efficient cell segmentation and identification on adaptive optics retinal images. *IEEE Trans Med Imaging*. 2021;40:2820–2831.
37. Liu J, Han Y-J, Liu T, Aguilera N, Tam J. Spatially aware dense-linkNet based regression improves fluorescent cell detection in adaptive optics ophthalmic images. *IEEE J Biomed Health Inform*. 2020;24:3520–3528.
38. Bower AJ, Liu T, Aguilera N, et al. Integrating adaptive optics-SLO and OCT for multimodal visualization of the human retinal pigment epithelial mosaic. *Biomed Opt Express*. 2021;12:1449–1466.
39. Liu J, Jung H, Dubra A, Tam J. Automated photoreceptor cell identification on nonconfocal adaptive optics images using multiscale circular voting. *Invest Ophthalmol Vis Sci*. 2017;58:4477–4489.
40. Curcio CA, Sloan KR, Kalina RE, Hendrickson AE. Human photoreceptor topography. *J Comp Neurol*. 1990;292:497–523.
41. Liu T, Jung H, Liu J, Droettboom M, Tam J. Noninvasive near infrared autofluorescence imaging of retinal pigment epithelial cells in the human retina using adaptive optics. *Biomed Opt Express*. 2017;8:4348–4360.
42. Lombardo M, Lombardo G, Lomoriello DS, Ducoli P, Stirpe M, Serrao S. Interocular symmetry of parafoveal photoreceptor cone density distribution. *Retina*. 2013;33:1640–1649.
43. Kay CN, Abramoff MD, Mullins RF, et al. Three-dimensional distribution of the vitelliform lesion, photoreceptors, and retinal pigment epithelium in the macula of patients with best vitelliform macular dystrophy. *Arch Ophthalmol*. 2012;130:357–364.


Investigative Ophthalmology & Visual Science

Downloaded from hwmaint.iovs.org on 04/24/2024